John J. Davenport, Jane Hodgkinson, John R. Saffell, and Ralph P. Tatam, "Noise analysis for CCD-based ultraviolet and visible spectrophotometry," Appl. Opt. 54, 8135-8144 (2015)

Noise analysis for CCD based ultra-violet and visible spectrophotometry

JJ Davenport [a], J Hodgkinson [a], JR Saffell [b] and RP Tatam [a]

a Engineering Photonics , Cranfield University Bedfordshire, MK43 0AL, UK
b Alphasense Ltd, 300 Avenue West, Skyline 120, Great Notley,
Essex CM77 7AA, UK

ABSTRACT

We present the results of a detailed analysis of the noise behaviour of two CCD spectrometers in common use, an AvaSpec-3648 CCD UV spectrometer and an Ocean Optics S2000 Vis spectrometer. Light sources used include a deuterium UV / Vis lamp and a UV LED including newly developed UV LEDs. Common noise phenomena include source fluctuation noise, photo-response non-uniformity (PRNU), dark current noise, fixed pattern noise (FPN) and read noise. These were identified and characterised by varying light source, spectrometer settings or temperature. A number of noise limiting techniques are proposed, demonstrating a best case spectroscopic noise equivalent absorbance (NEA) of 3.5×10^{-4}AU for the AvaSpec-3648 and 5.6×10^{-4}AU for the Ocean Optics S2000 both over a 30s integration period. These techniques can be used on other CCD spectrometers to optimise performance.

INTRODUCTION

Charged couple device (CCD) optical spectrometers are used in a wide range of fields, such as medicine, process control and scientific research. They are in common use in gas detection for compounds such as SO_2, NO_2 and the BTEX compounds (benzene, toluene, ethylbenzene and xylene) [1, 2, 3, 4].

CCD spectrometers are able to take rapid (sub millisecond) measurements and are highly versatile. Recently developed CCD spectrometers can be compact and portable and are able to

take measurements either open path or from an enclosed sample [1, 3]. At the same time recent developments in UV LEDs have opened the possibility of making comparisons of spectral measurements from a range of light sources.

An authoritative study into spectrometer noise was that of Rothman *et al* using a single beam molecular absorption spectrophotometer (EU-701A, GCA McPherson Corp.) [5]. It was still considered as such more than thirty years after publication [6, 7]. More recently studies have been carried out to characterise spectrometer developments such as diode arrays, photomultiplier tubes and CCDs [6, 8, 9, 10, 11].

In this study a characterisation is made of an AvaSpec-3648 CCD UV spectrometer and a Ocean Optics S2000 UV-Vis spectrometer. To the best of the author's knowledge noise performance of these spectrometers has not been reported before, but studies have been made of the similar AvaSpec-256 [12], Ocean Optics USB 4000 [11] and USB 2000 [9].

Ansko *et al* [12] have considered the stability of a CCD spectrometer and its stray light, for the purpose of measuring UV irradiance. Galban *et al* [11] have characterised noise in the Ocean Optics USB 4000 spectrometer, without explicitly identifying noise phenomena. The work of Zonios considers the noise phenomena of dark noise, fixed pattern noise (FPN) and stray light [9]. Here, we extend this analysis by identifying noise phenomena and also considering the effects of temperature and of the light source.

A spectroscopic measurement system consists of a broadband light source, light delivery / sample chamber and a spectrometer. In this study the noise behaviour of a the two spectrometers was characterised, taking advantage of new developments in CCD and LED technology, and making comparisons with a conventional light source (a deuterium lamp). A range of noise phenomena was identified including shot and fluctuation noise, dark current noise, read noise and pattern noise. Analysis of data taken at different temperatures and with different light sources has been used to explicitly identify and quantify noise from different sources.

Noise phenomena from other parts of the system such as sample chamber repositioning error play a significant role [5, 6], but this study predominantly deals with noise in the spectrometers themselves. Shot noise is included as it is fundamental to any light measurement system [9].

The extent of noise in the two spectrometers is discussed along with methods for limiting noise from specific sources. Finally we show the effect of these reductions on spectroscopic measurements and relate this to a noise equivalent absorbance (NEA).

PRINCIPLE OF OPERATION

The basic operation of a spectrometry system is a light source, a sample (gas in this case) and a spectrometer or spectral analyser as shown in Figure 1. Light from the light source passes through the sample, where different wavelengths are absorbed to different extents. The spectrometer then analyses the resulting spectrum to identify the sample's composition.

Figure 1: Basic operation of a spectrometry system. Light from the source passes through the sample and is analysed by the spectrometer.

The extent of absorption is given by the Beer-Lambert law (Equation(1)) [13] in which I_0 is the light intensity at wavelength λ measured with no sample present (mW). I is the intensity after passing through the sample (mW), σ is the absorption cross-section (cm^2), l is the path length of light passing through the sample (cm) and N is the sample molecular number density (cm^{-3}).

$$\frac{I(\lambda)}{I_0(\lambda)} = e^{-\sigma(\lambda)lN} \tag{1}$$

When the path length and sample concentration are constant, the *absorbance*, defined as $(I_0 - I) / I_0$, depends only on concentration of the absorbing species and its absorption cross-section. Each species has a unique spectrum of absorption cross-sections which allows it to be identified. Relevant regions of UV absorption cross-section spectra for gaseous formaldehyde and SO_2 are given in Figure 2 and Figure 3.

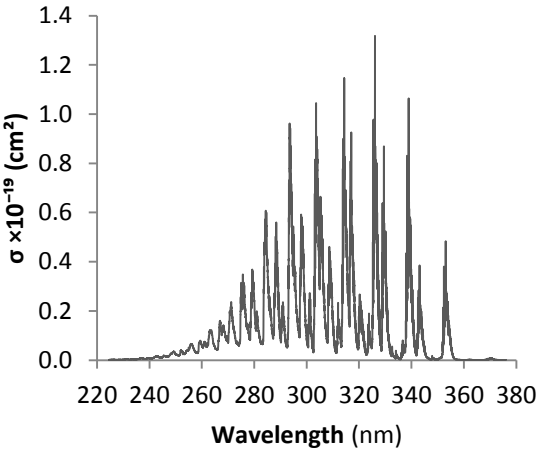

Figure 2: Selected region of the UV absorption cross-section for formaldehyde at 298 °K. Re-plotted from Meller *et al.* [14].

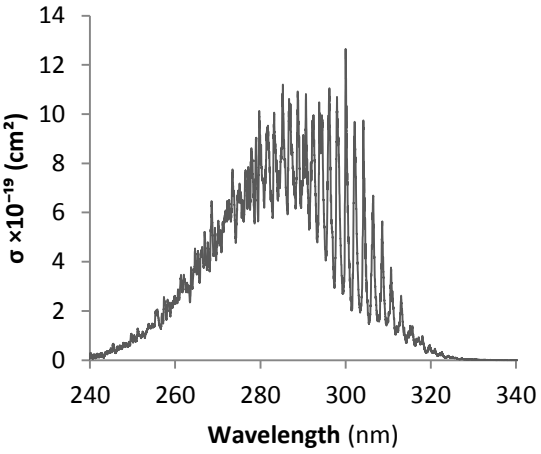

Figure 3: Selected region of the UV absorption cross-section for SO_2 at 298 °K. Re-plotted from Vandaele *et al*. [15].

Limits of detection can be quantified as the noise equivalent absorbance (NEA), given the dimensionless units AU (absorbance units), allowing instrumental techniques to be compared without reference to the specific target species. For estimates of noise and uncertainty in this study, we use the convention that $\langle n_e \rangle$ is the root mean squared (RMS) value of the variation of the number of electrons (one standard deviation).

Charge coupled devices (CCDs) are a common type of photo-detector based around generating a measureable voltage proportional to the number of incident photons over an array. They are used in a wide range of applications such as cameras and scientific and industrial light sensors as well as spectrometers. Some spectrometers use complementary metal–oxide–semiconductor (CMOS) arrays, which serve a broadly similar purpose. Spectrometers using CCD arrays tend to have a slightly faster readout and a slightly lower noise than CMOS arrays.

In a typical CCD array incident photons strike the depletion region which is a p-type semiconductor. If a photon's energy is greater than the semiconductor band gap and it is absorbed, it creates an electron-hole pair. In this example the electron remains in the depletion region while the hole is

removed by the ground electrode. The total number of photoelectrons that can be held in the depletion region is dependent on it dimensions and material and is known as the electron well capacity.

The second stage of CCD operation is transfer of charge across electron wells. The purpose is to collect charges from multiple pixels to be measured. Charge is transferred from well to well by manipulating their control voltages and it is this coupling of charge that gives the CCD its name [16]. The coupling architecture depends on the layout of the array.

The final stage of CCD operation is conversion of charge into a measurable voltage. This is carried out by a floating diode acting as a capacitor. It produces a voltage proportional to the CCD charge as described by Equation (2):

$$V = \frac{n_e G_{on}}{C} \tag{2}$$

where V is the voltage, G_{on} is the on-chip amplifier gain, and C is floating diode capacitance. CCDs are typically connected to further electronics that amplify the voltage and digitally encode it.

The total number of photoelectrons collected by a CCD pixel by a given incident intensity over a given time is described by Equation (3) [16]:

$$n_{pe} = A_D t_{int} R_e(\lambda) I(\lambda) \tag{3}$$

where A_D is the area of the pixel, t_{int} is the integration time and R_e is the spectral responsivity of the CCD pixel.

APPARATUS

This study used two spectrometers, an AvaSpec-3648 (Avantes AvaSpec-3648-USB2-SPU2) [17] and an Ocean Optics S2000 (Ocean Optics OEM S2000) [18]. Details of the spectrometers are given in

Table 1. A solarisation resistant optical fibre (Avantes FC-UV600-0.5-SR, 0.5m length, 600µm core radius) was used to deliver light to the spectrometers. Light was coupled into the fibre via UV grade fused silica lenses (40mm and 60mm focal length, both with 25mm diameter).

Table 1: Details of the two spectrometers used, as provided by the manufacturer

Parameter	**AvaSpec-3648**	**Ocean Optics S2000**
Spectral range	200 - 450nm	514 - 1,177nm
Spectral resolution	0.083nm	0.27 - 0.38nm
Pixels	3,648	2,048
Bit resolution	16 bit	16 bit
Total signal : noise	350:1	250:1
Dark noise	40 counts	3mV (10ms integration time)
Fixed pattern noise (FPN)	-	6mV (10ms integration time)
Photo-response non-uniformity (PRNU)	± 5%	5%
Read noise		3.5 counts RMS 20 counts peak-to-peak
Stray light	<0.04%	<0.10%

Diagrams of the internal optics of the two spectrometers are shown in Figure 4. The AvaSpec-3648 used the classical Czerny-Turner optical design [19] [20]. The Ocean Optics S2000 used a crossed-beam Czerny-Turner optical design [20]. In both layouts, light enters the spectrometer at the entrance aperture and the first spherical mirror collimates it onto the diffraction grating. Diffracted light then reaches the second spherical mirror which focuses it onto the CCD array. The profile of the spectrum can be found by the intensity of signal generated by the CCD pixels.

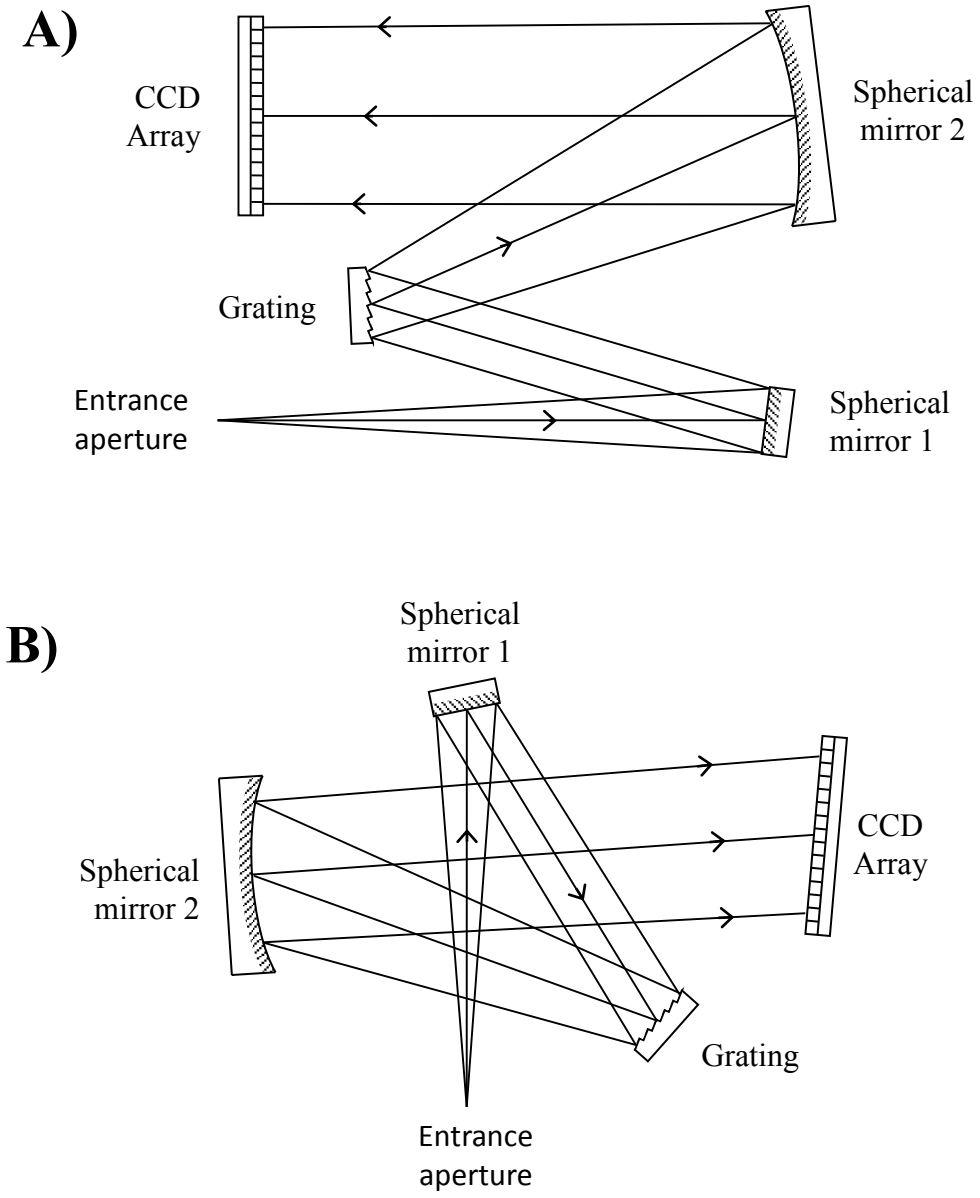

Figure 4: Diagrams of the internal optics of **A)** theAvaSpec-3648 and **B)** the Ocean Optics S2000. In both cases light entered the spectrometer at the entrance aperture and was collimated by the first mirror. It was then diffracted by the grating and directed by the second mirror onto the CCD array.

Three light sources were used for analysing the spectrometers. A UV lamp (Hamamatsu L10671 UV-Vis light source, incorporating an S2D2 deuterium lamp) [21] had a spectral range of 200nm to

1,600nm. The lamp was quoted as having a maximum wavelength drift of ±0.25nm per hour and a fluctuation of 0.004% (2×10^{-5}A.U.). A 340nm UV LED (SETi UVTOP335TO39BL) [22] had a quoted central wavelength of 340nm and an FWHM of 15nm. It was supplied with an internal parabolic mirror and a front ball lens (3.18mm radius). A 570nm visible LED (RS Components HLMPC515) [23] had a quoted central wavelength of 570nm and a 15nm FWHM. It was supplied in a cast plastic package with a semi-spherical front lens (2.5mm radius).

NOISE PERFORMANCE

For each potential source of noise, theoretical behaviour is described, followed by detailed results.

Shot noise and source fluctuation noise

Shot noise is caused by statistical variability in the rate of arrival of photons at the detector due to the quantised nature of light. Since photons arrive from their source independently of one another, shot noise is white noise and follows a Poisson distribution. It is described by the Schottky formula, Equation (4) [24] [25]:

$$\langle i_{sh} \rangle = \sqrt{2ei_{pe}\Delta f_e} \tag{4}$$

where i_{sh} is the shot noise current. e is the charge of an electron, i_{pe} is the current caused by photoelectrons and Δf_e is the noise equivalent bandwidth. In terms of the number of collected photoelectrons this can be given as:

$$\langle n_{pe} \rangle = \sqrt{2en_{pe}\Delta f_e} \tag{5}$$

Source fluctuation noise behaves in a similar statistical manner to shot noise, being white noise with a Poisson distribution in the rate of arrival of photons [24]. Together source fluctuation and shot noise

follow the generalised Equation (6). Unless the transmitted intensity is very low, source fluctuation noise tends to dominate shot noise.

$$\langle n_{pe} \rangle \propto \sqrt{n_{pe}} \tag{6}$$

The signal to noise ratio increases as the square root of signal intensity. It is not dependent on temperature and is a fundamental limit of any photon detection system. Increasing the integration time has the same effect on shot noise as increasing intensity, since the CCD chip has more time to gather photons.

The total number of electrons collected was varied to test shot noise and source fluctuation noise phenomena. Measurement time period was varied, thereby varying the number of photons arriving at the detector. Preliminary testing found no observed difference between use of a long integration time and summation over many measurements for the same total measurement period.

The fractional level of source fluctuation noise was found for the AvaSpec and Ocean Optics spectrometers using Equation (7):

$$\frac{\langle n_{pe} \rangle}{\sqrt{n_{pe}}} = \frac{\mathrm{stdev}(n_{pe})}{\sqrt{\mathrm{mean}(n_{pe})}} \tag{7}$$

where stdev(n_{pe}) is the standard deviation of photoelectron number and mean(n_{pe}) is the mean average of photoelectron number.

To compare both spectrometers, the deuterium source was used as its emission spanned the wavelength range of both. Measurements were taken with an integration time of 30ms in the spectrometer (see Figure 5) and the number of spectra averaged during post-processing was changed to vary the total measurement time. With a 30ms intergration time and the setup used for this, the peak intensity reaching the CCD array was close to the maximum measurable without saturating it.

For each pixel on the CCD, corresponding to a single wavelength "bin", the mean recorded intensity and its standard deviation were established, for repeated measurements taken at a single total integration time, to give the % source fluctuation noise for that pixel. Averages were taken of the % fluctuation for all active pixels and this average is shown in Figure 5, equivalent to the mean for single pixels. Theoretical predictions from Equation (6) are included with empirically fitted proportionality factors of 1.1 for the AvaSpec spectrometer and 1.47 for the Ocean Optics spectrometer.

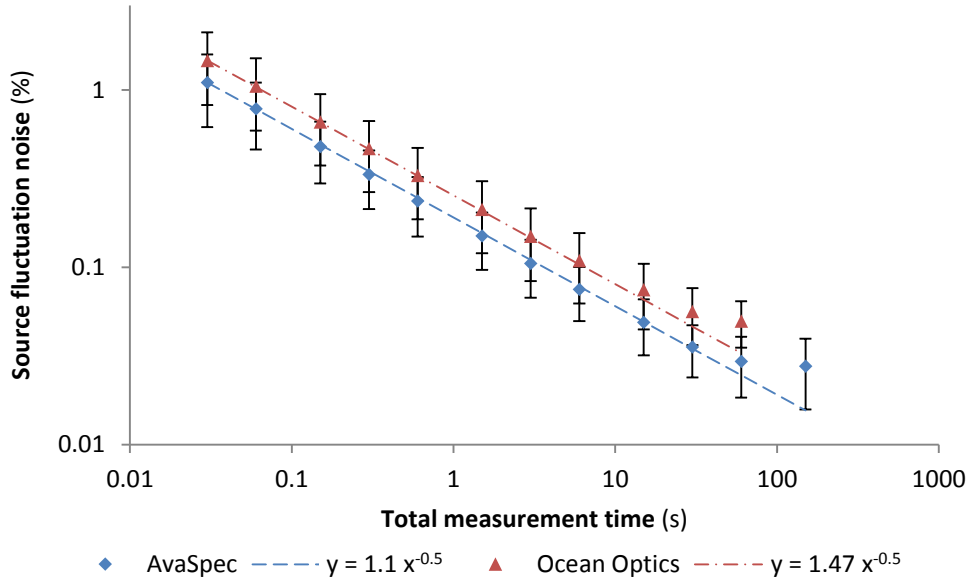

Figure 5: Effect of summing over multiple readings of source fluctuation noise from the two spectrometers, as mean noise at a single CCD pixel. Theoretical prediction from Equation (6) are included, with scaling factors fitted empirically to data between 0.03 and 30s.

The two spectrometers showed similar behaviour and good correspondence with theory for measurement times below approximately 30s. For measurement times above approximately 30s the source fluctuation noise diverges slightly from expected values. We attribute this to long-timescale drift effects (on the order of minutes) caused by slight temperature variations or mechanical instability.

While within errors of one-another, the results from the two spectrometers maintained a systematic difference in the mean fluctuation noise for any given integration and had different proportionality factors. The difference may have been caused by the different wavelength operational ranges of the two spectrometers. Variations in spectral emission mean that some pixels receive more photons in a given integration period, while others receive less, leading to the difference in fluctuation noise as $\sqrt{(n_{pe})}$. The 0.004% source fluctuation stated by the lamp manufacturer could not be measured with the signal from a single pixel but might be achievable as integrated fluctuation over the entire spectrum. The best mean single pixel level of noise recorded was 0.03% for the Avaspec and 0.04% for the Ocean Optics.

Dark current and fixed pattern noise

This section describes a number of effects which occur independently of the intensity of received light. In CCD chips, most dark current arises from thermal excitation of electrons in the semiconductor active material. It can also arise from background thermal radiation within the spectrometer, but this is probably not significant in the UV region.

The dark current generated by thermal excitation of electrons is given by [16]:

$$n_{dark} = \frac{J_D A_D t_{int}}{q} \tag{8}$$

where A_D is the area of the detector, t_{int} is the integration time of the spectrometer and J_D is the dark current density given by [16]:

$$J_D \approx k_B \, exp\left(-\frac{E_G}{\alpha_G k_B T}\right) \tag{9}$$

where E_G is the semiconductor band gap, α_G is the dark current factor for the semiconductor material ($1 \leq \alpha_G \leq 2$) , k_B is the Boltzmann constant and T is temperature in Kelvin.

The intensity of background radiation is given by [26]:

$$I_{bg}(\lambda, T) = \frac{2\pi hc^2}{\lambda^5} \cdot \frac{1}{e^{hc/k_B T\lambda} - 1} \tag{10}$$

where h is the Planck constant and c is the free space speed of light. Blackbody radiation tends to be strongest in the IR region for bodies at standard temperature.

The mean dark current is constant for fixed conditions but the noise on individual readings is expected to follow a Poisson distribution. Hence, dark current noise has the same relationship with signal magnitude as shot noise, described by as Equation (6).

Fixed pattern noise (FPN) arises from differences in the mean dark current between pixels, generally caused by variations in the detector area or the dark current density. It does not generally vary with time, and is present irrespective of signal level [16]. These variations tend to be caused by imperfections in CCD manufacture and so FPN remains constant from one measurement to the next. FPN is unique to each spectrometer, and must therefore be identified, but when this has been done it can simply be subtracted from measurements [9].

In order to characterise signal-independent noise phenomena, measurements were taken under dark conditions. Dark current was measured at a range of integration times for both spectrometers and the results are shown in Figure 6. For each data point, counts were averaged across all pixels to control for FPN. Error bars were estimated from the standard deviations of ten measurements.

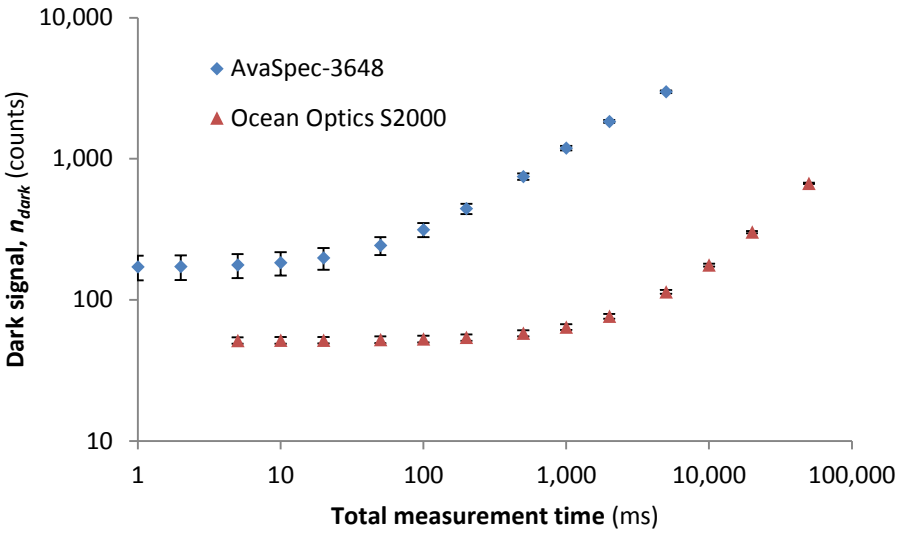

Figure 6: Change in average dark signal with integration time for the two spectrometers. Both spectrometers show a region where dark signal increases with integration time as expected, and a region where it remains constant, attributed to read noise. Data points represent the mean dark current across all pixels. 1 and 2ms integration times were not available for Ocean Optics spectrometer.

Both sets of data show a region where dark current increases with integration time as expected, because the CCD chips had more time to gather dark signal. However, for low integration times there is a region where dark current is constant. This was attributed to read noise, which is independent of integration time (see Section 5.4.5). The minimum dark current level was 170±30 counts for the AvaSpec-3648 and 52±3 counts for the Ocean Optics S2000.

Dark current noise was tested in the same manner as for shot noise and source fluctuation noise, by varying the total measurement time and thereby the number of photons collected. The results for the AvaSpec and Ocean Optics spectrometers are shown in Figure 7. Theoretical predictions from Equation (6) are included with empirically fitted proportionality factors of 35 for the AvaSpec spectrometer and 2.87 for the Ocean Optics spectrometer. Errors were estimated from the standard deviation between pixels.

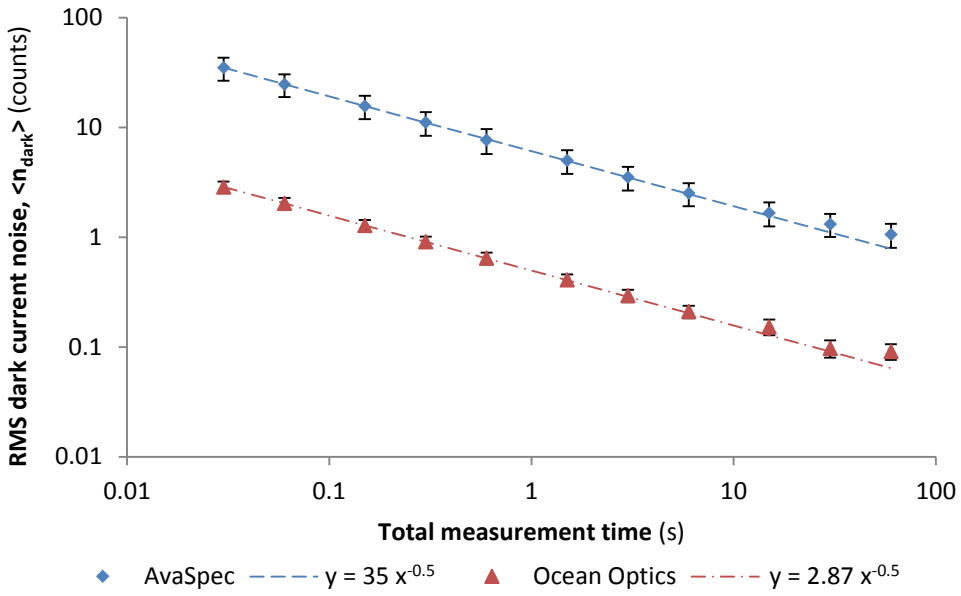

Figure 7: Effect of averaging over multiple measurements on dark current noise from the two spectrometers. Theoretical prediction from Equation (6) are included, with scaling factors empirically to data between 0.03 and 30s ($y = 35\ x^{-0.5}$ for the AvaSpec-3648 and $y = 2.87\ x^{-0.5}$ for the Ocean Optics S2000).

The behaviour of the two spectrometers was very similar to that seen for shot noise and source fluctuation noise. Both spectrometers showed good correspondence with theory for measurement times below 30s. As before, noise values for measurement times above 30s diverge slightly from theoretical values, attributed again to drift effects.

The FPN for the two spectrometers is presented in Figure 8 and Figure 9. This data was taken under dark conditions. The patterns were very repeatable between measurements, the AvaSpec-3648 and the Ocean Optics S2000 having RMS variation between measurements of 0.5% and 0.15% respectively. The AvaSpec-3648 spectrometer data shows three statistically significant peaks at 278nm, 369nm and 409nm. They were dominated by other noise sources for signals above 11,000 counts. They may have been due to stray light or possibly some electronic source.

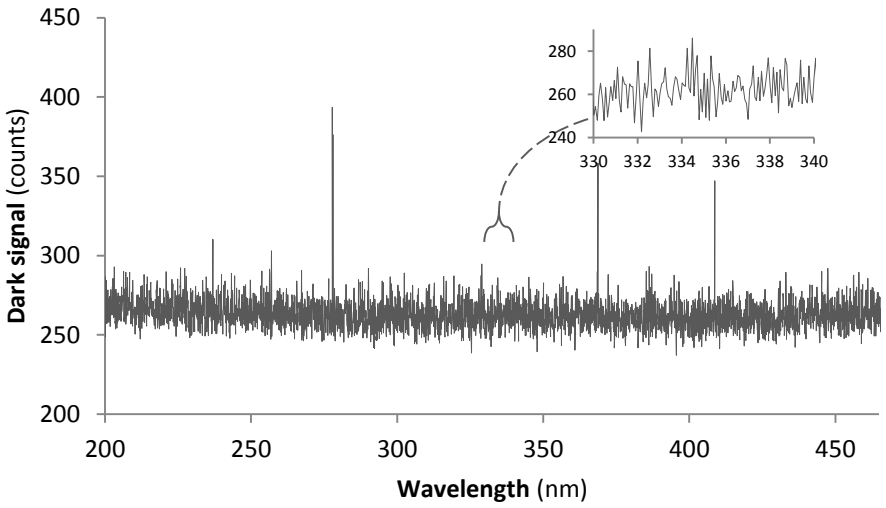

Figure 8: AvaSpec-3648 FPN measured with an integration time of 30ms and averaged over 10,000 readings. Between 200 and 450nm the FPN had an average value of 263 counts and an RMS variation of 9.4 counts. Outliers can be seen at 278nm, 369nm and 409nm. Average RMS variation between measurements was 0.5%. The insert shows a typical section of the data at full resolution (0.083nm).

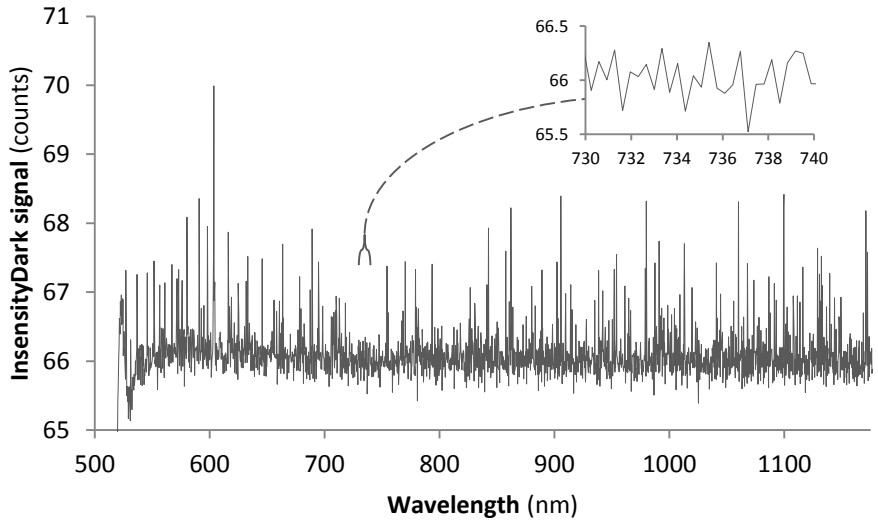

Figure 9: Ocean Optics S2000 FPN measured with an integration time of 30ms and averaged over 10,000 readings. Between 514 and 1,177m the FPN had an average value of 66 counts and an RMS variation of 0.38 counts. Average RMS variation between measurements is 0.15%. The insert shows a typical section of the data at full resolved (0.27 – 0.38nm).

The effect of temperature on FPN was found by placing the spectrometer in an environmental chamber at a series of elevated temperatures. The entrance aperture was covered to provide dark conditions. At least 1 hour was allowed between temperature changes to allow the system to reach thermal equilibrium. The test was run several times with different integration times, varying the number of averages in order to keep the total integration period of each measurement the same. The FPN variation was then determined as the RMS deviation from the mean across all pixels.

A sample of the results from the AvaSpec spectrometer is shown in Figure 10. They did not behave as expected. According to Equation (8) and Equation (9), the dark current of each pixel should increase with temperature, resulting in an increase in the magnitude of both dark current and of the of FPN variations on that current. As can be seen in Figure 10, the dark current decreased with increasing temperature whereas the FPN increased (observable in the difference in "noise" between 25 and 30°C).

In the extreme case, this effect decreased the signal to zero counts, at which point it could not be measured. Some of the data taken at 35°C can be seen to fall to zero counts in Figure 10. At 40°C, only the highest values could be measured above zero counts. In a private communication with the manufacturer, this behaviour was identified as a voltage offset on the detector [27] from which the signal baseline decreased with increasing temperature. The effect was seen in both spectrometers and is assumed to have a similar underlying cause in each.

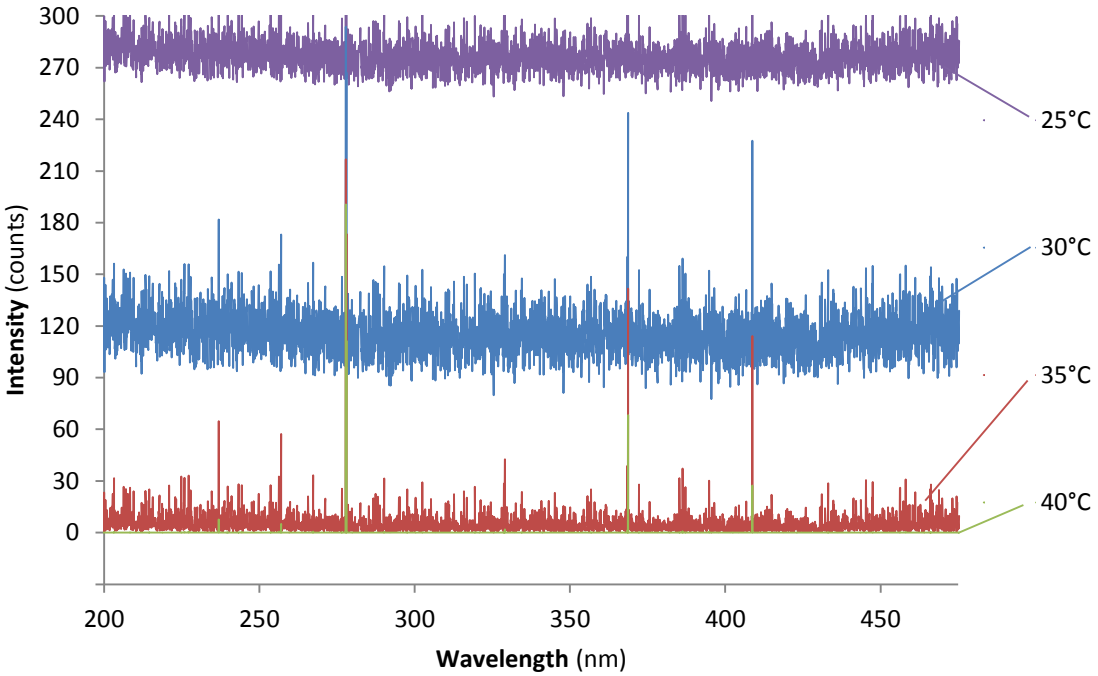

Figure 10: Sample FPN of the AvaSpec spectrometer measured at different temperatures. The position decreases with increasing temperature instead of increasing as expected, attributed to a voltage offset on the detector. Not all of the 25°C data is shown in this graph.

Data showing a significant number of points at zero counts was therefore removed from the subsequent analysis. Figure 11 and Figure 12 show that the FPN variation of the two spectrometers increased with temperature as expected. Results from a range of integration times are included, demonstrating a variation in FPN as expected. In both spectrometers the voltage offset dominated dark current for high temperature and low integration time measurements, and meaningful FPN variation figures could not be found.

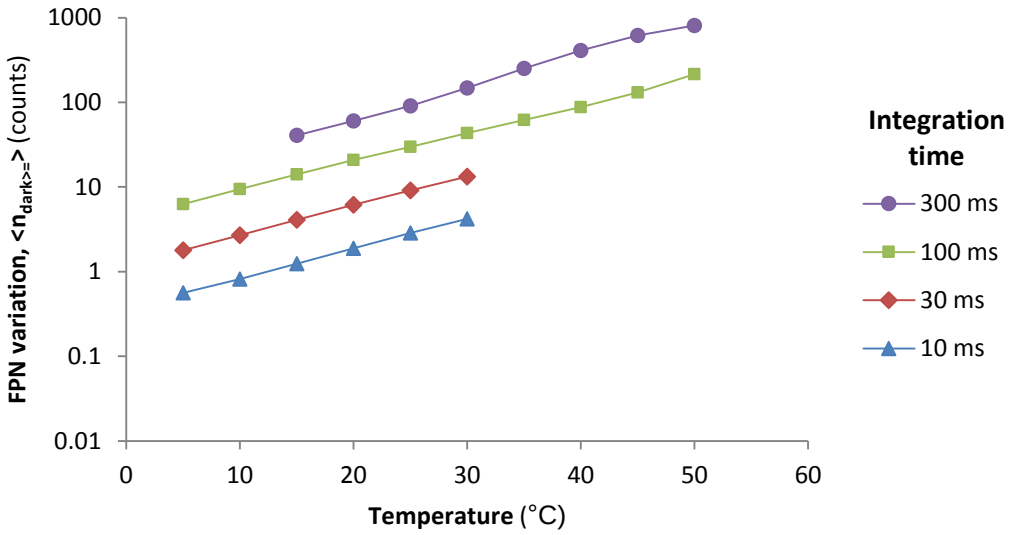

Figure 11: AvaSpec spectrometer temperature dependence of FPN, found as RMS variation of dark current and over a range of integration times. FPN variation increases with increasing temperature as expected.

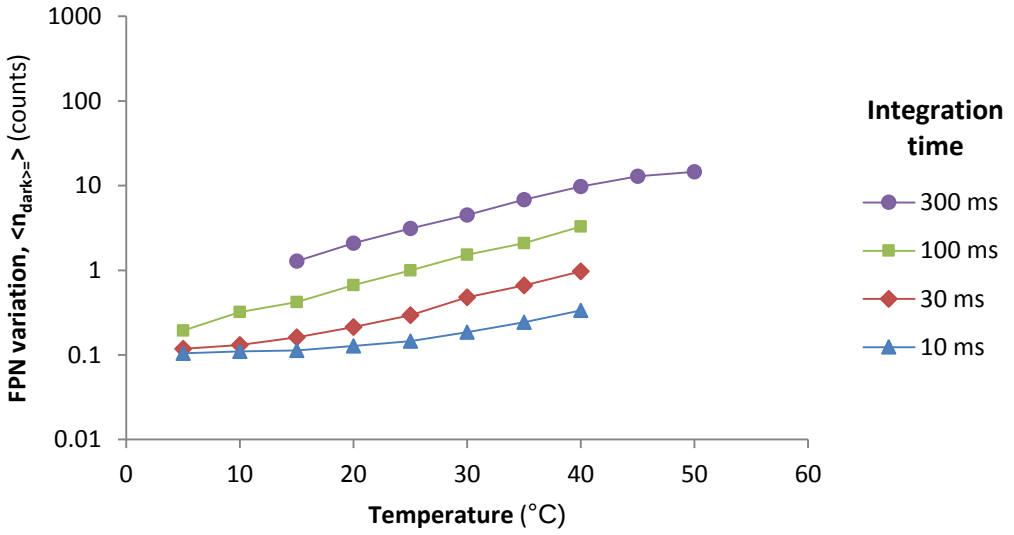

Figure 12: Ocean Optics spectrometer temperature dependence of FPN, found as RMS variation of dark current and taken over multiple integration times. It behaved similarly AvaSpec spectrometer but FPN variation did not decrease below about 0.1 counts due to the effect of count digitisation following averaging.

It was important when using either spectrometer that the signal did not become unreadable as a result of high temperature operation and so longer integration times should be used for low-signal, high-temperature measurements.

Read noise

This category includes noise phenomena that occur when charge carriers in the CCD are converted into electrical signals, as described in Section 5.1. CCDs are typically connected to further electronics that amplify the voltage, referred to as off-chip amplifiers [16], which also cause read noise. The final phenomenon included in this category arises from voltage analogue-to-digital conversion.

(i) Reset noise arises from thermodynamic variations in the resetting voltage at the sense node capacitor, between readings [28]. It is described by Equation (11), where C is the sense node capacitance [16]:

$$\langle n_{reset} \rangle = \frac{\sqrt{k_B T C}}{q} \tag{11}$$

(ii) The on-chip amplifier converts charge packets to current [29] and has noise described by Equation (12), where V_{on} is the noise voltage after the on-chip amplifier [16]:

$$\langle n_{on\text{-}chip} \rangle = \frac{C}{qG_{on}} V_{on} \sqrt{\Delta f_e} \tag{12}$$

(iii) Off-chip amplifier noise has a very similar form, being described by Equation (13), where G_1 is the off-chip amplifier gain and V_{off} is the noise voltage after the off-chip amplifier [16].

$$\langle n_{off\text{-}chip} \rangle = \frac{C}{qG_{on}G_{off}} V_{off} \sqrt{\Delta f_e} \tag{13}$$

(iv) Finally, quantisation noise is produced by analogue to digital conversion and follows Equation (14), where N_{well} is the electron well capacity and N_{bit} is the bit resolution of the converter [16]:

$$\langle n_{ADC} \rangle = \frac{N_{well}}{2^{N_{bit}}\sqrt{12}} \tag{14}$$

Read noise is not dependent on integration time as it only occurs when the signal is taken from the CCD. The total read noise can be found by combining the different components as in Equation (15). The read noise is generally expected to be fixed for any given pixel.

$$\langle n_{read} \rangle^2 = \langle n_{reset} \rangle^2 + \langle n_{on-chip} \rangle^2 + \langle n_{off-chip} \rangle^2 + \langle n_{ADC} \rangle^2 \tag{15}$$

As read noise occurs once per measurement, it is difficult to reliably identify it. Other noise phenomena in signal transfer systems or in computer or data logging devices may well behave in the same way. Distinguishing between different types of read noise can also be difficult. In practice, however, a single value can be given for a spectrometer which describes all noise phenomena behaving in this manner.

Figure 6 shows the dark current of the Avaspec and Ocean Optics spectrometers, measured at a range of integration times. Both spectrometers show behaviour consistent with read noise. Dark current levels off with decreasing integrations times instead of continuing to decrease as expected for random dark noise. This gave a minimum dark current attributed to read noise of 171±34 counts for the AvaSpec-3648 and 51.5±3 counts for the Ocean Optics S2000.

Photo-response non-uniformity

Photo-response non-uniformity (PRNU) is a variation in responsivity from one pixel to the next, caused by variations in detector area or spectral responsivity (see Equation (3)). Like FPN, it is caused by imperfections in CCD manufacture and is unique to each spectrometer [9]. PRNU is most significant for high intensity measurements and bright conditions, while FPN is most significant in

low intensity measurements and dark conditions. PRNU responds proportionally to signal intensity, and so is difficult to distinguish from variations in source intensity across the measured spectrum.

PRNU is described by Equation (16), where *U(λ)* is the fixed pattern ratio (a scaling factor that applies to each pixel independently [16]).

$$\langle n_{prnu} \rangle = U(\lambda) n_{pe} \tag{16}$$

An estimation of PRNU was found for two independent light sources (deuterium lamp and UV or visible LED) by subtracting the assumed 'true' spectra. The latter was found by using a seven term polynomial equation, fitted to the measured data. It allowed a smooth shape to be fitted to the measured spectra whilst ignoring sub-nm wavelength structure. It did not account for any spectrally narrow features of the source, or spectrally broad PRNU features. Values were then normalised for power due to the linear relationship of PRNU with signal (from Equation (3)).

The AvaSpec spectrometer was used with the deuterium lamp and again with 340nm LED to estimate PRNU. The Ocean Optics spectrometer also used the deuterium UV lamp and the 570nm LED, as the 340nm LED was out of its spectral range. Samples of the results from the two spectrometers are shown in Figure 13 and Figure 14.

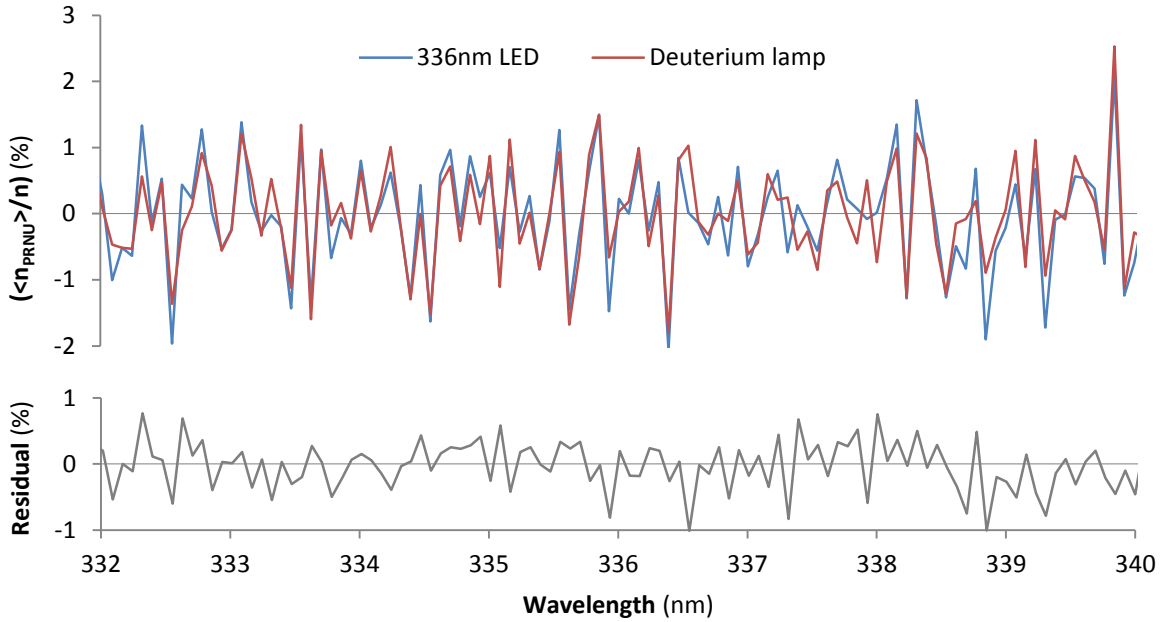

Figure 13: Comparison of PRNU of the AvaSpec spectrometer measured using the 340nm LED and the deuterium lamp. Percentages are given in terms of total signal.

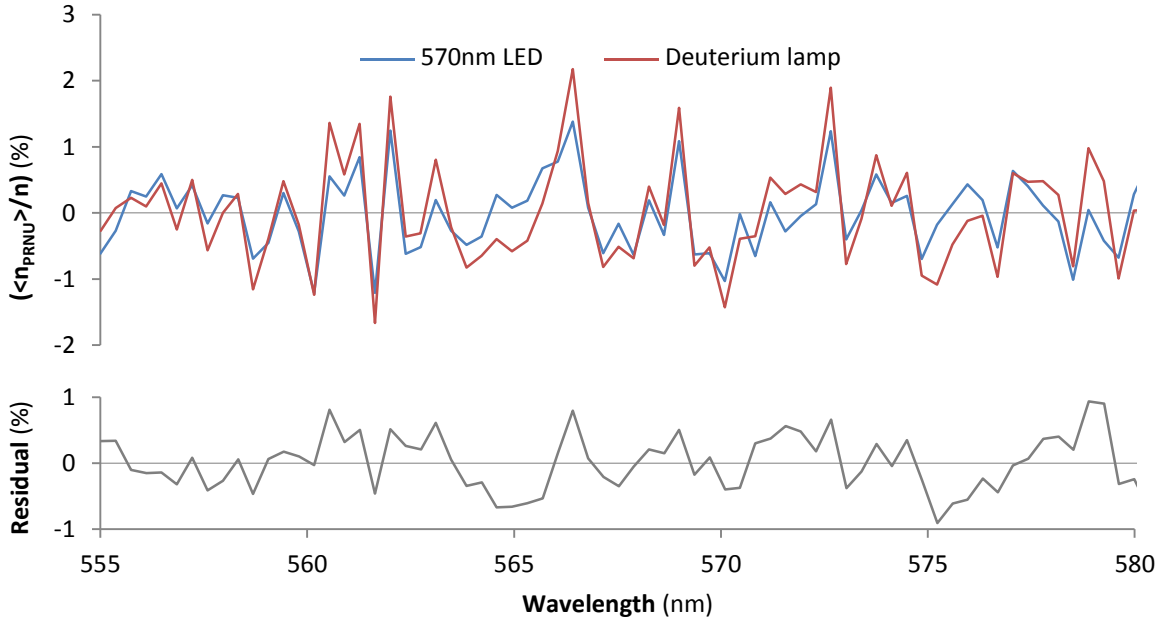

Figure 14: Comparison of PRNU of the Ocean Optics spectrometer with the 570nm LED and the deuterium lamp. Percentages are given in terms of total signal.

The average RMS PRNU in these regions was found to be 0.6±0.2% for the AvaSpec-3648 and 0.54±0.17% for the Ocean Optics S2000. The majority of the errors on these values come from the residual differences between measurements made using different sources, therefore it is not easy to distinguish between PRNU and systematic variations in source intensity. The residual is the worst case PRNU, assuming that it is responsible for all differences between the two data sets and not spectral differences between sources.

PERFORMANCE OPTIMISATION

The following methods are proposed for limiting a number of the noise phenomena identified above.

Increased sampling

Noise phenomena that vary randomly with time such as shot noise, source fluctuations and dark current noise can be decreased by increased sampling using one of two methods:

(i) Longer integration times within the CCD itself. Higher integration time can increase dark current and can cause saturation for high-intensity signals.

(ii) Averaging over multiple CCD readouts. A lag time of up to 7ms between readouts must be considered, and therefore this method will only provide an advantage for integration times longer than 10ms. Use of multiple readouts may also cause an increase in read noise.

In this study a total measurement time of 30s was achieved by using a 30ms integration time and averaging over 1,000 measurements. Improvements from increased sampling were limited by long-term drift effects, which came to dominate for longer term measurements.

Temperature control

Many of the noise phenomena described in this study were temperature-dependent. Variations in temperature could affect the dark current noise and cause shifts in the baseline of measurements. Temperature stability is therefore highly desirable during spectrometer measurements.

The room temperature of the main laboratory used for this study varied between 22 and 24ºC. For most tests this was found to be sufficiently stable. For some particularly sensitive measurements it was necessary to control the temperature with an environmental chamber (±0.1ºC).

Care was taken to avoid decreasing the temperature to the point of damaging the apparatus, for example by causing condensation or even ice crystals to form. Spectrometers were therefore kept above 0°C. Also, when the signal was very low, the voltage offset described in Section 5.4.4 could dominate the signal. This would render measurements impossible. Consequently, temperature should be kept at 40°C or below except in high signal cases.

Dark current correction

Two methods were identified to correct for dark current and FPN.

(i) Dynamic dark correction is an automatic function that can be implemented on a spectrometer to correct for dark current in real time. It subtracts the same dark current from readings across the full wavelength range and so makes no correction for variations due to pattern noise. It was therefore best suited to measurements of rapidly changing conditions with short integrations times. This method was generally avoided as the spectrometer did not record the level of dark noise subtracted, and because conditions were generally kept stable.

(ii) The second method was to record the dark current of the spectrometer across all pixels in advance and manually subtract it from readings. This was the preferred method. It corrects for both dark current and FPN. As described above, dark current is not constant with temperature and so it needed to be recorded in conditions as close to measurement conditions as possible. Generally, this involved recording dark noise immediately before or immediately after experiments. Where temperature was controlled, pre-recorded dark current values could be used.

PRNU scaling

Figure 13 gives the measured PRNU of a selected part of the spectrum of the AvaSpec-3648. Its response to increasing signal intensity was linear according to by Equation (16). Once the PRNU has been characterised, it becomes possible to scale measured signal to account for it. As stated above, PRNU is unique to each spectrometer and so must be determined before any scaling is undertaken, requiring at least two light sources to isolate it from source spectral variation. A source with a smoothly varying spectrum, such as a blackbody source, would enable definitive measurement of PRNU, but this would be difficult to implement for the UV spectrum.

For spectroscopic measurements, a comparison is made between the measured spectrum of a light source with a sample of gas present and without it. It is therefore not necessary to isolate spectral variation of the spectrometer and the source, as both should remain constant between readings and the two could be scaled together.

Optimisation results

Noise phenomena identified in this study fell into two main categories: those that were dependent on the external signal and those that were not, and would apply to dark conditions. Table 2 gives a summary of noise phenomena in these two categories including initial levels measured and levels after

methods of limitation have been employed. Controlled figures assume the 30ms integration times and 1,000 averages mentioned earlier.

Table 2: Noise values before and after controls for the AvaSpec-3648 and Ocean Optics S2000

Phenomenon	**Avaspec-3648 before controls**	**Avaspec-3648 after controls**	**Ocean Optics S2000 before controls**	**Ocean Optics S2000 after controls**
Signal-dependent				
PRNU	0.60%	0.19%	0.54%	0.17%
Shot and source fluctuation noise	1.10% (0.03s period)	0.035% (30s period)	1.47% (0.03s period)	0.056% (30s period)
Total	1.25%	0.19%	1.56%	0.18%
Signal-independent				
FPN	9.43 counts	1.32 counts	0.38 counts	0.097 counts
Dark current noise	34.9 counts	1.06 counts	2.86 counts	0.091 counts
Total	36.2 counts	1.69 counts	2.89 counts	0.13 counts

In general signal-independent phenomena, such as dark current noise, FPN and read noise, will dominate for low intensity measurements. Signal-dependent phenomena, such as source fluctuation noise and PRNU, will dominate for high intensity measurements. Stray light is more difficult to define quantitatively and so does not fall into either category. Noise figures are given as a percentage of signal for signal-dependent phenomena and as an absolute count rate for signal-independent phenomena. Total noise of each type is found by taking the square root of the sum of squared values.

For spectroscopic measurements, the limit of detection is dominated by signal-dependant noise phenomena as they involve small deviations from the signal of a high intensity light source. Hence the optimum NEA for the AvaSpec-3648 is 1.9×10^{-3}AU and the NEA for the Ocean Optics S2000 is

1.8×10^{-3}AU. In many cases the light source will remain constant and so it will not be necessary to distinguish to PRNU from variations in source spectral intensity. The combined variation can then be cancelled, improving optimum NEA to 3.5×10^{-4}AU for the AvaSpec-3648 and 5.6×10^{-4}AU for the Ocean Optics S2000.

CONCLUSIONS

In this paper we have taken advantage of new developments in CCD and LED technology to characterise and compare the noise performance of a pair of CCD spectrometers. A range of noise phenomena were identified and quantified for these spectrometers. A number of recommendations have been made for minimising the noise of the spectrometer. They can be applied to other CCD based spectrometers as a general performance optimising method.

Source fluctuation noise and dark current noise occur randomly and can be limited by increasing the sample size, either by using longer integration times or by averaging over multiple measurements. These increase the time for a measurement to be taken which allow long term drift effects to dominate. Suspected read noise dominated over dark current noise for integration times lower than 20ms for the AvaSpec-3648 and lower than 500ms for the Ocean Optics S2000. As with shot noise, dark current noise can be reduced by increasing total integration time. It can also be reduced by controlling temperature.

Fixed pattern noise is a pattern of dark noise that is constant between measurements and unique to each spectrometer. Fixed pattern noise was observed to decrease with increasing temperature for both spectrometers. This was not expected and is understood to be caused by a temperature-dependent voltage offset in the electronics. As fixed pattern noise remains constant for given conditions, it can be subtracted from results during post processing. Photo-response non-uniformity is a variation in responsivity between pixels. Both spectrometers show PRNU that was measurable by making comparisons of signal from two independent light sources.

A number of noise limiting techniques are proposed, including increased integration periods, temperature control, dark correction and PRNU scaling. With a 30s integration period and assuming a constant light source, these provide a best case spectroscopic NEA of 3.5×10^{-4}AU for the AvaSpec-3648 and 5.6×10^{-4}AU for the Ocean Optics S2000.

REFERENCES

[1] M. Degner and H. Ewald, "Low cost sensor for online detection of harmful diesel combustion gases in the UV-Vis region," *Proceedings of the SPIE,* vol. 6198, pp. 619806-619817, 2006.

[2] M. Hu, T. Y. Wang, Z. F. Qiao, B. Geng and X. H. Xiao, "Research on VOC Concentration Detection by Photoelastic Modulation Infrared Spectrum Absorption Methods," *Spectroscopy and Spectral Analysis,* vol. 31, no. 12, pp. 3232-3235, 2011.

[3] D. Bernini, F. Caucia and M. Boiocchi, "Application of the Vis-NIR Avaspec-2048 portable automatic spectrometer to distinguish GEM quality materials," *Neues Jahrbuch Fur Mineralogie-Abhandlungen,* vol. 185, no. 3, pp. 281-288, 2009.

[4] J. Hodgkinson and R. P. Tatam, "Optical gas sensing: a review," *Measurement Science & Technology,* vol. 24, no. 1, p. 012004, 2013.

[5] L. D. Rothman, S. R. Crouch and J. D. Ingle, "Theoretical and Experimental Investigation of Factors Affecting Precision in Molecular Absorption Spectrophotometry," *Analytical Chemistry,* vol. 47, no. 8, pp. 1226-1233, 1975.

[6] J. Galban, S. de Marcos, I. Sanz, C. Ubide and J. Zuriarrain, "Uncertainty in modern spectrophotometers," *Analytical Chemistry,* vol. 79, no. 13, pp. 4763-4767, 2007.

[7] D. A. Skoog, S. Crouch, D. M. West and F. J. Holler, Fundamentals of analyitical chemistry, 8th ed, Brooks/Cole: Pacific Grove, CA, 2004.

[8] S. R. Springston and A. J. Sedlacek, "Noise characteristics of an intrumental particle absorbance technique," *Aerosol science and technology,* vol. 41, pp. 1110-1116, 2007.

[9] G. Zonios, "Noise and stray light characterization of a compact CCD spectrophotometer used in biomedical applications," *Applied Optics,* vol. 49, no. 2, pp. 163-169, 2010.

[10] J. Nieke, M. Solbrig and A. Neumann, "Noise contributions for imaging spectrometers," *Applied Optics,* vol. 38, no. 24, pp. 5191-5194, 1999.

[11] J. Galban, S. de Marcos, I. Sanz, C. Ubide and J. Zuriarrain, "CCD detectors for molecular absorption spectrophotometry. A theoretical and experimental study on characteristics and performance," *Analyst,* vol. 135, no. 3, pp. 564-569, 2010.

[12] I. Ansko, K. Eerme, S. Latt, M. Noorma and U. Veismann, "Study of suitability of AvaSpec array spectrometer of solar UV field measurements," *Atmospheric Chemistry and Physics,* vol. 8, no. 12, pp. 3247-3152, 2008.

[13] J. D. Ingle and S. R. Crouch, Spectrochemical Analysis, London: Prentice Hall, 1988.

[14] R. Meller and G. K. Moortgat, “Temperature dependence of the absorption cross sections of formaldehyde between 223 and 323 K in the wavelength range 225-375 nm,” *Journal of Geophysical Research-Atmospheres,* vol. 105, pp. 7089-7101, 2000.

[15] A. C. Vandaele, C. Hermans and S. Fally, “Fourier transform measurments of SO2 absorption cross sections: II. Temperature dependence in the 29000-44000cm-1 (227-345 nm) region,” *Journal of Quantitative Spectroscopy & Radiative Transfer,* vol. 110, pp. 2115-2126, 2009.

[16] G. C. Holst, CCD Arrays, Cameras, and Displays, Washington: SPIE Press, 1996.

[17] Avantes AvaSpec-3648-USB2-SPU2, *Technical Data Sheet,* Avantes, Apeldoorn, The Netherlands, 2010.

[18] Ocean Optics OEM S2000, *Technical Data Sheet,* Ocean Optics, Dunedin, Florida, USA, 2011.

[19] K. Lee, K. P. Thompson and J. P. Rolland, “Broadband astigmatism-corrected Czerny–Turner spectrometer,” *Optics Express,* vol. 18, no. 22, pp. 23378-23378, 2010.

[20] J. M. Simon, M. A. Gil and A. N. Fantino, “Czerny-Turner monochromator: astigmatism in the classical and in the crossed beam dispositions,” *Applied Optics,* vol. 25, no. 20, pp. 3715-3720, 1986.

[21] L. Hamamatsu S2D2 UV-Vis Light Source, *technical data sheet,* Hamamatsu, Hamamatsu, Japan, 2010 .

[22] SETi UVTOP335, *technical data sheet,* Sensor Electronic Technology Inc., Columbia, USA.

[23] T-1 3/4 Super Ultra-Bright LED Lamps, *technical data sheet,* RS Components, Corby, UK.

[24] J. D. Winefordner, R. Avni, T. L. Chester, J. J. Fitzgerald, L. P. Hart, D. J. Johnson and F. W. Plankey, “A comparison of signal-to-noise ratios for single channel methods (sequential and multiplex) vs multichannel methods in optical spectroscopy,” *Spectrochimica Acta Part B-Atomic Spectroscopy,* vol. 31(1), pp. 1-19, 1976.

[25] S. Engelberg, “The Wiener-Khinchin theorem and applications,” in *Random signals and noise; a mathematical introduction*, Boca Raton, CRC Press, 2006, pp. 110-114.

[26] E. Hecht, Optics, Second Edition, Reading, Massachusetts: Addison-Wesley Publishing Company, 1987.

[27] Private conversation with Neville Davies, Senior Applications Scientist, Account Manager, Ocean Optics, 2013.

[28] J. Hynecek, “Spectral Analysis of Reset Noise Observed in CCD Charge-Detection Circuits,” *IEEE Transactions on Election Devices,* vol. 37, no. 3, pp. 640-647, 1990.

[29] P. Centen, “CCD On-Chip Amplifiers: Noise Performance versus MOS Transistor Dimensions,” *IEEE Transactions on Eletron Devices,* vol. 38, no. 5, pp. 1206-1216, 1991.

Noise analysis for CCD-based ultraviolet and visible spectrophotometry

Davenport, John

2015-08-17

John J. Davenport, Jane Hodgkinson, John R. Saffell, and Ralph P. Tatam. Noise analysis for CCD-based ultraviolet and visible spectrophotometry, Applied Optics, Vol 54, 2015, pp. 8135-8144
http://dx.doi.org/10.1364/AO.54.008135